Resource

Chemistry & Biology

Systematic Mapping of Kinase Addiction Combinations in Breast Cancer Cells by Integrating Drug Sensitivity and Selectivity Profiles

Graphical Abstract

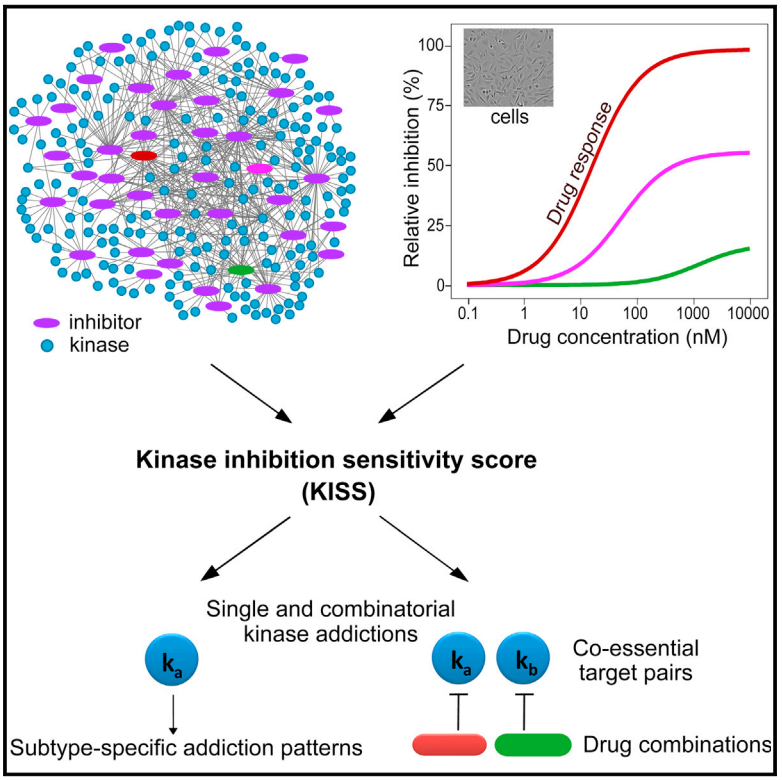

Highlights

- Chemical systems biology tool for mapping kinase signal addictions in cancer cells
- Makes use of a network of interactions between kinase inhibitors and their targets
- We detected subtype-specific addiction patterns across 21 breast cancer cell lines
- We identified both co-essential target pairs and synergistic drug combinations

Authors

Agnieszka Szwajda, Prson Gautam, Leena Karhinen, ..., Jing Tang, Krister Wennerberg, Tero Aittokallio

Correspondence

tero.aittokallio@fimm.fi (T.A.), krister.wennerberg@fimm.fi (K.W.)

In Brief

Szwajda et al. developed a systems biology approach that integrates drug selectivity and sensitivity profiles to identify pharmacologically actionable signal addictions, both single and combinatorial, in given cancer cells. Such druggable molecular vulnerabilities may lead to stratified therapeutic strategies in various cancer subtypes.

Szwajda et al., 2015, Chemistry & Biology 22, 1144–1155
August 20, 2015
http://dx.doi.org/10.1016/j.chembiol.2015.06.021

CellPress

Chemistry & Biology
Resource

Systematic Mapping of Kinase Addiction Combinations in Breast Cancer Cells by Integrating Drug Sensitivity and Selectivity Profiles

Agnieszka Szwajda,[1] Prson Gautam,[1] Leena Karhinen,[1] Sawan Kumar Jha,[1] Jani Saarela,[1] Sushil Shakyawar,[1] Laura Turunen,[1] Bhagwan Yadav,[1] Jing Tang,[1] Krister Wennerberg,[1,*] and Tero Aittokallio[1,*]
[1]Institute for Molecular Medicine Finland, FIMM, University of Helsinki, 00014 Helsinki, Finland
*Correspondence: tero.aittokallio@fimm.fi (T.A.), krister.wennerberg@fimm.fi (K.W.)
http://dx.doi.org/10.1016/j.chembiol.2015.06.021

SUMMARY

Chemical perturbation screens offer the possibility to identify actionable sets of cancer-specific vulnerabilities. However, most inhibitors of kinases or other cancer targets result in polypharmacological effects, which complicate the identification of target dependencies directly from the drug-response phenotypes. In this study, we developed a chemical systems biology approach that integrates comprehensive drug sensitivity and selectivity profiling to provide functional insights into both single and multi-target oncogenic signal addictions. When applied to 21 breast cancer cell lines, perturbed with 40 kinase inhibitors, the subtype-specific addiction patterns clustered in agreement with patient-derived subtypes, while showing considerable variability between the heterogeneous breast cancers. Experimental validation of the top predictions revealed a number of co-dependencies between kinase targets that led to unexpected synergistic combinations between their inhibitors, such as dasatinib and axitinib in the triple-negative basal-like HCC1937 cell line.

INTRODUCTION

Successful examples of molecularly targeted anticancer drug treatments exist only for a few cancer types that are driven by druggable oncoproteins (Huang et al., 2014). Cancer sequencing efforts have revealed that individual driver mutations may target multiple signaling pathways, and each cancer patient may exhibit a unique combination of mutations that are sufficient to perturb these pathways (Vandin et al., 2012). This extensive mutational heterogeneity poses increasing challenges for the current target-based drug development and repurposing approaches that try to connect recurrent genomic alterations to acquired cellular vulnerabilities (Garraway and Lander, 2013). Importantly, even when the critical driver genes can be identified, these often turn out to be clinically not actionable (i.e. there is no targeting drug available for clinical use) or pharmacologically "undruggable" (i.e. it is impossible to develop a drug against the gene product or its variant). Furthermore, genes that are not altered at the sequence level may also play an essential role in the disease progression, hence providing additional therapeutic opportunities (Pe'er and Hacohen, 2011). For instance, cancer sequencing studies have not found frequent mutations in protein kinases, despite the known addiction of many cancer cells to kinase signaling (Torkamani et al., 2009; Tyner et al., 2013). Therefore, complementary strategies are needed to pinpoint the functional consequences of perturbations, which may help to prioritize the most potent and clinically actionable drugs and their target combinations for each individual patient.

Pharmacological perturbation screens using broadly targeted chemical libraries of bioactive small molecules enable systematic and direct phenotypic assays for functional investigation of the druggable vulnerabilities in individual cancer cell types or patient-derived samples (Heiser et al., 2012; Pemovska et al., 2013, 2015). However, most chemical inhibitors of kinases and other common cancer targets are relatively non-specific, leading to a number of "off-target" effects that may either cause adverse side effects or improve the therapeutic response (Xie et al., 2012). Such polypharmacological effects complicate the identification of signal addictions directly from the drug-response phenotypes. Furthermore, the exponentially increasing number of possible drug-target combinations is beyond the experimental and financial capacity of even automated high-throughput screening technologies, and translates into a need for integrated experimental-computational approaches that enable deconvoluting the underlying signaling cascades behind individual drug-response profiles. Network-based strategies can naturally take into account the complex interactions between drugs and their cellular targets, and so-called network pharmacology approaches are increasingly being developed for many applications (Hopkins, 2008; Tang and Aittokallio, 2014; Zhao and Iyengar, 2012). However, systematic approaches that make use of comprehensive drug response profiling to reveal druggable dependencies in individual cancer samples have remained rare (Tyner et al., 2013).

In the present work we developed and tested a network pharmacology approach, which integrates cell-based drug sensitivity profiling with biochemical target selectivity information for systematic identification of druggable molecular vulnerabilities in given cancer cells. This approach enables the identification of both individual kinase target addictions (i.e. essential kinase signals) and combinatorial co-dependencies between kinase pairs and synthetic lethal type interactions (i.e. co-essential kinase

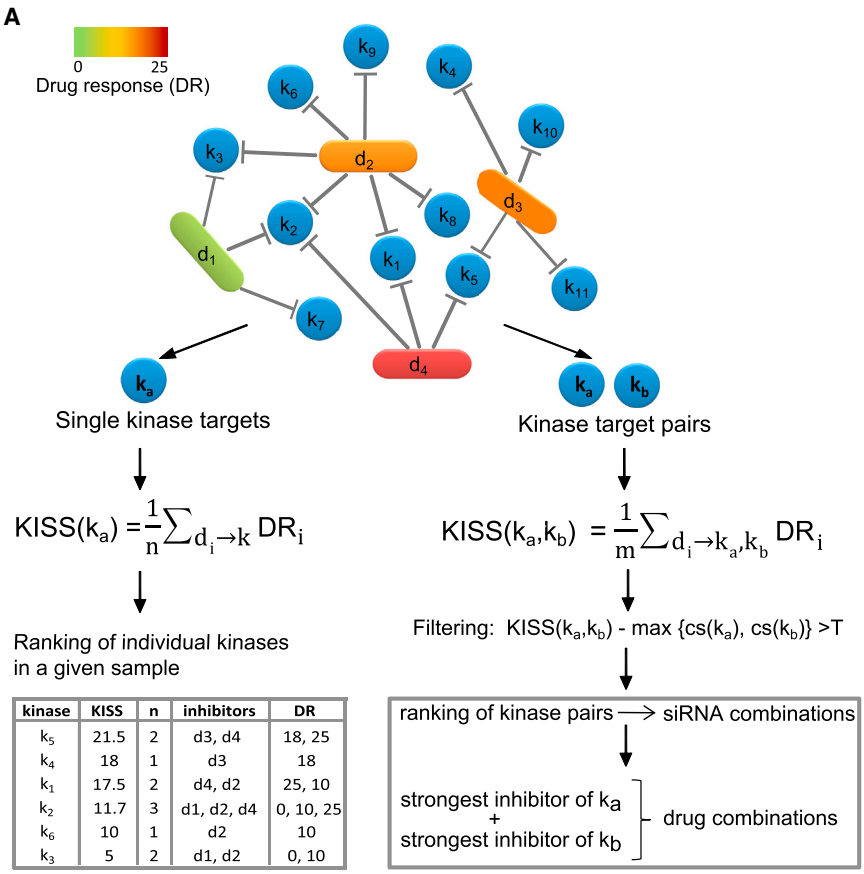

kinase	KISS	n	inhibitors	DR
k_5	21.5	2	d3, d4	18, 25
k_4	18	1	d3	18
k_1	17.5	2	d4, d2	25, 10
k_2	11.7	3	d1, d2, d4	0, 10, 25
k_6	10	1	d2	10
k_3	5	2	d1, d2	0, 10

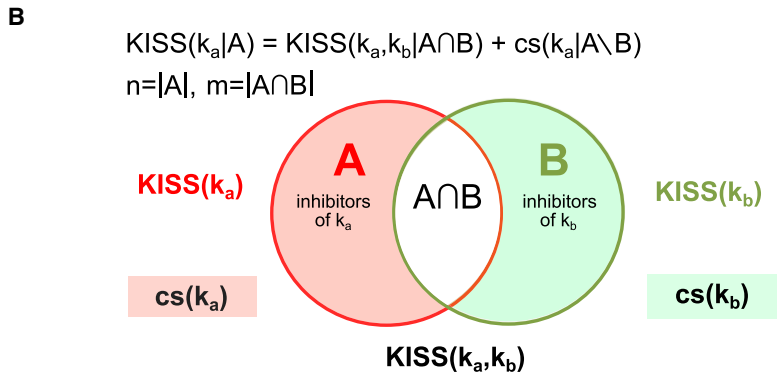

Figure 1. Schematic Illustration of the Single and Combinatorial Kinase Inhibition Sensitivity Score

(A) Left: Single kinase inhibition sensitivity score (KISS) ranks each kinase (k) in the context of a given drug-target network based on the average drug response (DR) over the subset of its potent inhibitors (n). Single KISS enables one to prioritize pharmacologically actionable kinase signal addictions in individual cancer cell samples for experimental validation. Right: The KISS concept was extended to ranking kinase pairs (k_a, k_b) based on their average combinatorial effect over the subset of inhibitors targeting both of the kinases (m). Combinatorial KISS enables one to identify a synthetic lethal type of target pairs, which may lead to synergistic drug combinations between their inhibitors (see B for the rationale of the filtering step). Experimental testing of the combinatorial KISS predictions was carried out here by simultaneous siRNA-based silencing of the highly ranked kinase pairs and by combinations of drugs that show most potency as inhibitors of k_a and k_b.

(B) Relationships between the single and combinatorial KISS defined using set-theoretic operations among the set of inhibitors. Using this notation, the cardinality of the set A is n and the cardinality of the intersection between A and B is m. The complement score (cs) of k_a or k_b is defined as the average response over the inhibitors that belong to the difference between sets A and B or B and A, respectively (the shaded portions).

signals). The integrated approach makes use of the polypharmacological effects of compounds in terms of utilizing both their unique and shared on- and off-targets in the deconvolution of the underlying kinase signaling pathways. As a proof-of-principle case study, we used triple-negative breast cancer (TNBC), a highly aggressive and heterogeneous class of breast cancer, with currently no targeted treatments available, mainly due to the lack of known single drivers (Grigoriadis et al., 2012). Therefore, TNBC serves as a highly challenging disease model to identify druggable molecular addictions and combinatorial co-dependencies in a cell type-specific manner. Although we focused here on breast cancer cell lines and kinase inhibitors, the experimental-computational approach is also widely applicable to other target families and cancer types, as well as to patient-derived cell samples in clinical applications.

RESULTS

Kinase Inhibition Sensitivity Score for Predicting Single and Combinatorial Molecular Addictions

We implemented an experimental-computational target deconvolution approach, dubbed the kinase inhibition sensitivity score (KISS), which maps kinase inhibitor sensitivity and selectivity profiles onto a drug-target network (Figure 1A). Our computational algorithm ranks the individual kinases according to their likelihood of being essential for the growth of a particular cancer cell (Pemovska et al., 2013; Yadav et al., 2014). The basic assumption behind the KISS addiction scoring model is that the increased sensitivity of a cancer cell to a given drug compound implies that its molecular targets are jointly and/or individually essential for the survival of the cancer cell, whereas drug treatment insensitivity implies that the particular cell is not addicted to the targets of the particular compound.

Formally, KISS for a given kinase target is calculated as the average drug response over the subset of its potent inhibitors (Figure 1A, left). We extended this concept also to kinase target pairs,

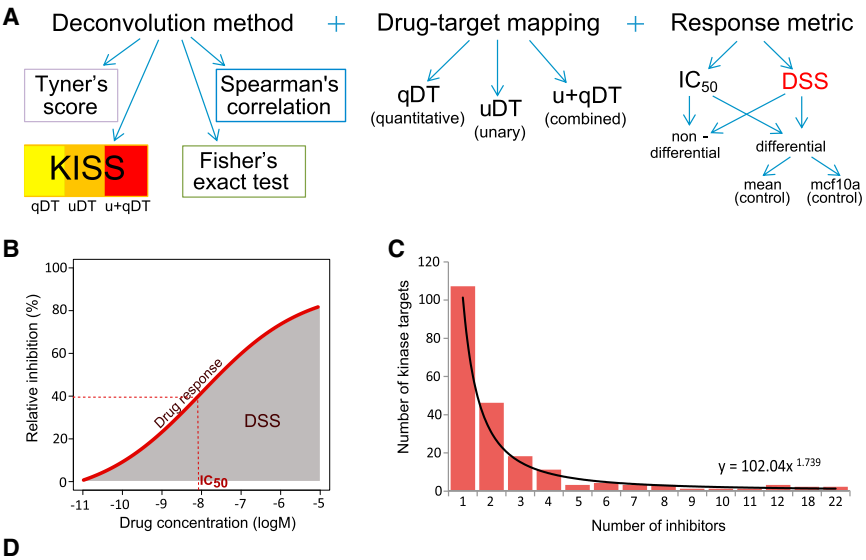

D

		CELL LINE	BT474	SKBR3	MDAMB453	T47D	MCF7	MDAMB453	DU4475	
COMBINATION		DRIVER	ERBB2	ERBB2	ERBB2	PIK3CA	PIK3CA	PIK3CA	BRAF	MEDIAN
KISS	qDT	dDSSmean	1	1	1	15	1	4	1	1
KISS	uDT	dDSSmean	1	1	1	NA	NA	NA	30	1
KISS	u+qDT	dDSSmean	2	2	1	21	2	7	21	2
KISS	qDT	dDSSmcf10a	1	2	15	2	1	3	1	2
Fisher	qDT	dDSSmcf10a	1	2	8	2	3	3	3	3
Fisher	qDT	dDSSmean	4	3	2	4	27	4	1	4
Fisher	qDT	dIC50mean	4	3	2	9	83	89	3	4
Fisher	qDT	DSS	2	2	1	6	6	8	6	6
KISS	u+qDT	dDSSmcf10a	6	9	11	29	9	12	9	9
KISS	uDT	dDSSmcf10a	6	9	10	NA	NA	NA	72	9.5
KISS	qDT	DSS	1	2	19	11	1	20	19	11
KISS	uDT	DSS	11	12	13	NA	NA	NA	17	12.5
KISS	qDT	dIC50mcf10a	2	9	40	15	51	52	4	15
KISS	qDT	IC50	1	8	24	11	16	55	63	16
Fisher	qDT	dIC50mcf10a	7	17	36	5	28	36	13	17
KISS	uDT	dIC50mean	26	7	10	NA	NA	NA	43	18
KISS	qDT	dIC50mean	18	6	6	58	56	80	14	18
KISS	uDT	IC50	39	10	11	NA	NA	NA	27	19
Tyner	qDT	IC50	2	2	10	304	19	341	193	19
KISS	uDT	dIC50mcf10a	11	23	26	NA	NA	NA	79	24.5
KISS	u+qDT	DSS	25	26	31	16	2	25	47	25
Spearman	qDT	dDSSmean	4	54	27	47	6	9	243	27
Fisher	qDT	IC50	2	12	56	12	28	56	44	28
KISS	u+qDT	IC50	143	13	29	24	30	64	97	30
Spearman	qDT	dDSSmcf10a	55	32	163	9	2	4	167	32
Spearman	qDT	DSS	23	26	49	38	16	35	304	35
KISS	u+qDT	dIC50mcf10a	10	28	37	59	106	104	34	37
Spearman	qDT	dIC50mcf10a	57	13	228	38	50	42	63	50
KISS	u+qDT	dIC50mean	119	10	12	75	96	106	61	75
Spearman	qDT	IC50	12	13	167	88	51	120	251	88
Spearman	qDT	dIC50mean	10	7	140	213	94	82	221	94

Figure 2. KISS and Quantitative Drug-Target Mappings Improve the Identification of Known Breast Cancer Drivers

(A) Systematic evaluation of cancer addiction identification approaches, each based on a combination of a deconvolution method, a type of drug-target mapping, and a drug-response metric as input.

(B) Drug sensitivity score (DSS, Table S1) is based on the integration of the area under the dose-response curve (Yadav et al., 2014), and combines several response parameters such as relative half-maximal inhibitory concentration (IC_{50}).

(C) The number of inhibitors that target a given number of kinases among the tested drug collection of 40 inhibitors and 205 kinase targets. Dissociation constant (K_d) values (Davis et al., 2011) were used to define here the quantitative drug-target (qDT) mappings according to expert filtering (Table S3). The solid curve corresponds to a power function.

(D) Ordering of the 31 tested combinations according to the median rank of known drivers used as positive controls. Color coding of the KISS-based combinations corresponds to the different types of drug-target mappings (see A). NA marks those combinations in which the driver was absent in the particular type of drug-target interaction data. Red font indicates combinations based on DSS. Table S4 gives the full results from each combination.

by means of combinatorial KISS, which enables the prediction of such kinase pairs whose simultaneous inhibition leads to increased cell death (Figure 1A, right). To focus on the synthetic lethal type interactions, we retained only those target pairs for which the combinatorial effect was markedly higher than that originating from the inhibitors targeting only one of the kinases (Figure 1B; see also Experimental Procedures). It was hypothesized that tracing back the inhibitors behind such co-essential target pairs could lead to unbiased prediction of synergistic drug combinations.

KISS Enabled the Prediction of Context-Specific Drivers in Heterogeneous Breast Cancer Cells

In this proof-of-principle study, we examined the sensitivity of 21 breast cancer cell lines to a panel of anticancer compounds using the drug sensitivity and resistance testing platform (Pemovska et al., 2013) (Table S1). Specifically, 15 of the cell lines represented TNBC subtypes, three were ER and PR positive, two were Her2 positive, and one was Her2, ER, and PR positive (Table S2). To evaluate the relative performance of KISS across these breast cancer cell lines, we ranked the kinase targets based on a representative set of computational target deconvolution methods (Figure 2A): Tyner's score (Tyner et al., 2013), Fisher's test (Wei et al., 2012), and Spearman's correlation (Tran et al., 2014) (see Experimental Procedures). Drug response was quantified either as half-maximal inhibitory concentration (IC_{50}) or by using the drug sensitivity score (DSS) (Yadav et al., 2014) (Figure 2B). Quantitative drug-target selectivity profiles were available from a biochemical assay (Davis et al., 2011) for 40 kinase inhibitors in our compound collection (Table S3), whose target distribution followed the power function (Figure 2C). We also tested whether targets extracted from public drug databases (KEGG, Therapeutic Target Database, and DrugBank) could improve the identification of kinase addictions (Figure 2A). Each of these combinations of a target deconvolution method, a drug-target mapping, and a drug response metric gave rise to a separate ranking of kinase targets (Table S4).

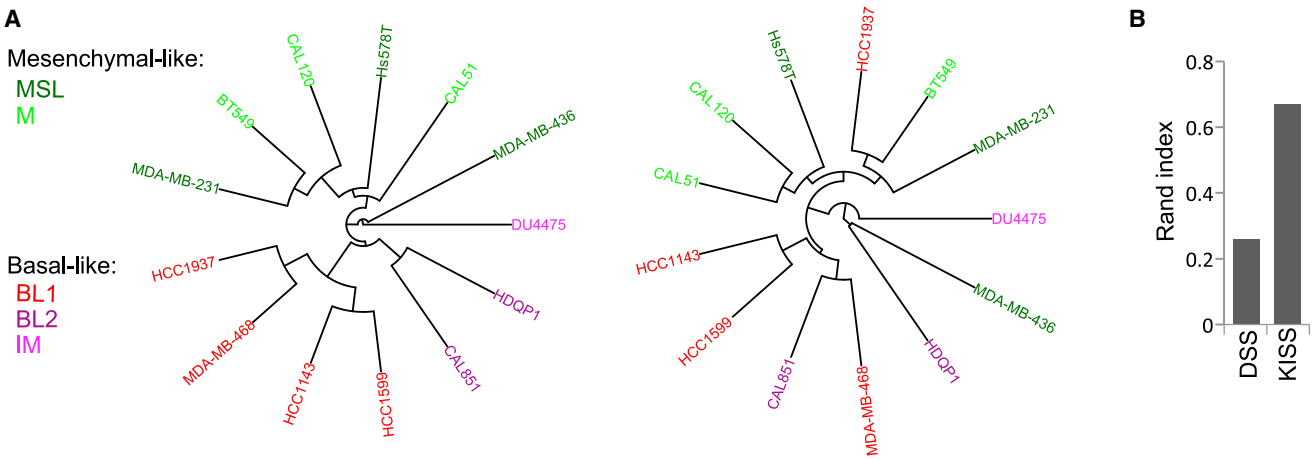

Figure 3. KISS-Based Clustering Reveals TNBC Subgroups in Agreement with Patient-Based Subtypes

(A) Unsupervised cluster solutions based on KISS (left) and DSS (right) were compared with the five subgroups established in TNBC patient tumors based on their transcriptomic profiling: basal-like 1 (BL1), basal-like 2 (BL2), immunomodulatory (IM), mesenchymal (M), and mesenchymal stem-like (MSL). For each of these patient-derived subgroups, a set of representative TNBC cell lines was previously determined (Lehmann et al., 2011). The cell lines overlapping with our cell line collection were used here in the cluster evaluation (Table S2 provides the characterization of all cell lines). The luminal androgen receptor (LAR) subgroup was excluded due to the lack of androgen receptor antagonists in our kinase inhibitor panel. See also Figure S1 for KISS-based clustering of all tested cell lines.
(B) Adjusted R and index for the quantitative assessment of agreement between the KISS- and DSS-based cluster solutions with the patient-derived TNBC subtypes.

The systematic evaluations demonstrated the improved ability of the KISS-based combinations to predict known kinase drivers of breast cancer cell lines (ERBB2 in BT474 and SKBR3, BRAF in DU4475 as well as PIK3CA/PI3Kα in MCF7 and T47D; Figure 2D). Strikingly, all of the top four rankings of these positive controls were based on KISS and DSS, and 11 out of 12 top rankings were based on the DSS, indicating that the DSS metric provides an improved means beyond the standard IC_{50} to elucidate cancer cell addictions. As was expected, the differential version of DSS improved the prediction results when the aim was to find selective addictions that are specific to a given cancer cell. However, merging unary drug-target interactions with quantitative target selectivity profiles did not lead to improvements in the predictive accuracy, suggesting that taking into account negative drug-target interactions has an important role in the driver predictions. The KISS version that utilizes differential DSS and quantitative drug-target profiles turned out to be the overall best combination across all the tested cell lines and their known drivers (Figure 2D). This version was therefore used in the further evaluations and applications of the KISS approach.

KISS-Based Cancer Cell Clustering Closely Resembled Patient-Derived TNBC Subtypes

Unsupervised clustering of the breast cancer cell lines based on their KISS profiles revealed three major clusters with distinct kinase signal addictions (Figure 3A). To test whether the KISS-based functional clustering could identify breast cancer subtypes similar to those observed in patient tumors, we compared the clusters derived from the KISS profiles with the classification obtained using genome-wide molecular profiles from 587 TNBC cases (Lehmann et al., 2011). It was found that the KISS-based clustering agreed better with the patient-derived TNBC subtypes, compared with that using the drug response profile alone (Figure 3B).

Notably, the KISS profiles of MDA-MB-436 and DU-4475 did not cluster together with any other TNBC cell lines (Figure 3A). This is because the experimentally validated top kinase predictions in MDA-MD-436, including GLK/MAP4K3, KHS/MAP4K5, TYK1/LTK, RON, MET, and IRAK4 (Figure 4), were distinct from the set of significant addiction scores in the other mesenchymal-like cell lines ($p < 0.05$, permutation-based test). Similarly, DU-4475, which represents the immunomodulatory subtype (Lehmann et al., 2011), did not cluster together with the other basal-like cell lines due to its validated addictions to RAF family and SRMS kinases (Figure 4). It also had common predicted drivers with mesenchymal-like CAL51 and Hs578T cell lines, including CAMKs, GRKs, and PKNs, which had very low KISS values in all the basal-like cell lines (Table S4; Figure S1). These results indicate that the KISS profiles provide additional information beyond the established breast cancer cell types.

Predicted Kinase Addiction Patterns Showed Variability between and within Established Cell Types

In addition to the known oncogenic drivers, the KISS-based rankings suggested novel cell line-specific druggable addictions. To experimentally test a set of novel addiction predictions, we initially focused on the HDQP1 cell line, which was predicted to be strongly addicted to CSK, BMX, HCK, and IRAK and to ephrin receptor tyrosine kinases (Figure 4; Table S4). Since its addiction profiles partially overlapped with those of CAL51 and Hs578T, we tested a selection of top addiction predictions in these three TNBC cell lines using both siRNA-based kinase knockdowns and an independent set of compounds that inhibit the predicted kinases but were not used in the model construction or KISS predictions (Figure 4). In general, we were able to confirm a number of the predicted hits by an independent compound and/or siRNA validation assays (Figure 4; Table S5).

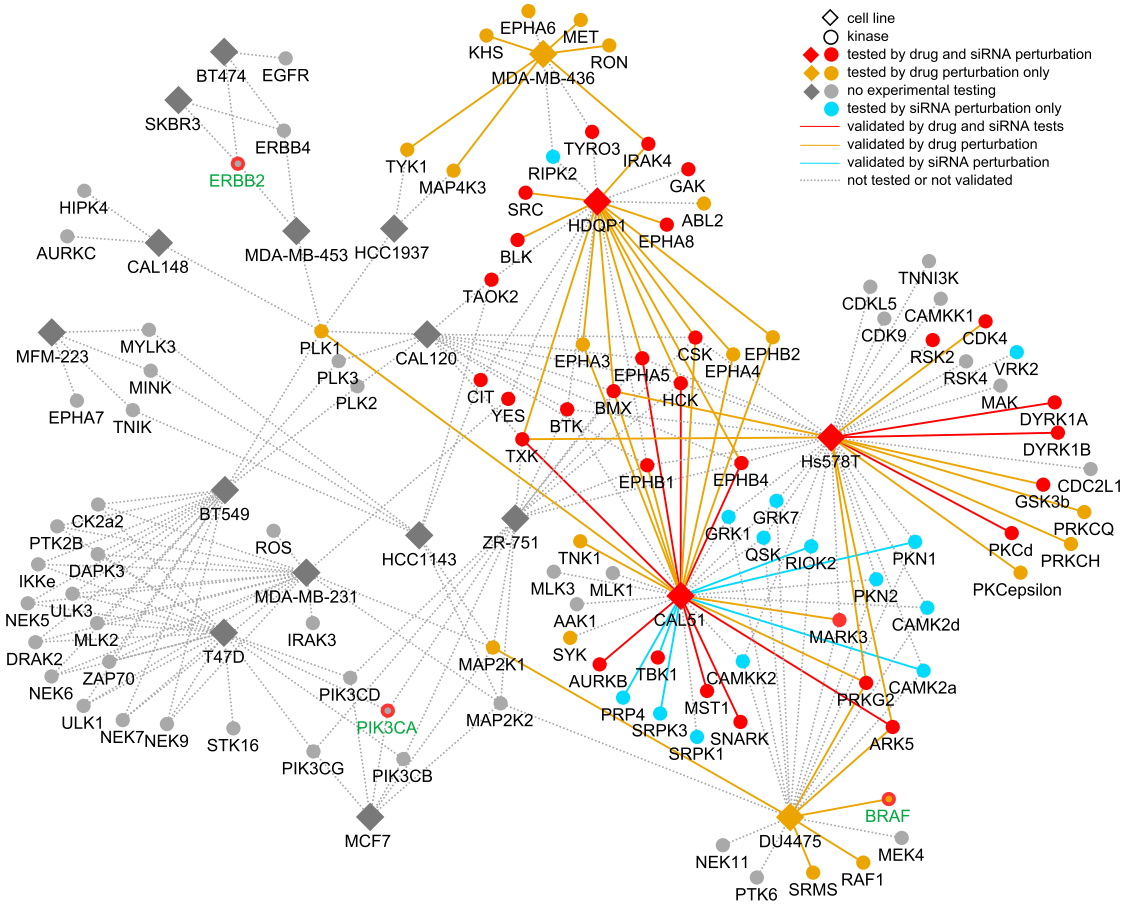

Figure 4. Unique and Shared Kinase Addiction Patterns among the Heterogeneous Breast Cancer Cell Lines

The kinase addiction network was constructed among the statistically significant KISS values in separate cell lines ($p < 0.06$, permutation test). The node color represents the type of experimental evaluation performed for the particular kinase prediction in a given cell line. The edge color represents the result of the validation experiment(s) utilizing either independent drugs (i.e. targeted kinase inhibitors not among the FIMM compound panel) and/or siRNA-based kinase knockdown (i.e. silencing of the predicted kinase target using three siRNAs per kinase in three replicates). Kinases that are known to be drivers of the cell lines are marked with a red node border and a green kinase label. The independent siRNA and drug validations were considered positive if the average siRNA inhibition from the two most effective siRNA sequences was above 35% and the drug sensitivity score was above 7, respectively. Table S5 gives the full validation data.

Taking CAL51 as an example TNBC cell line, our experimental validations confirmed the importance of multiple AMP-activated protein kinase-related kinases, such as ARK5 (NUAK1), SNARK (NUAK2), and MARK3 (Figure 4; Table S5). In addition, CAMK2A, PKN1, RIOK2, PRP4, and SRPK3 were experimentally confirmed by growth inhibition following their knockdown by siRNAs. Both the siRNA and compound perturbation results supported the essentiality of ARK5, SNARK, and MST1, as well as dasatinib targets EPHA5, EPHB4, HCK, and TXK. Notably, many of the KISS-predicted addictions have been previously implicated in cancers (Table S5). The number of kinase predictions confirmed either in our validation experiments or in other studies provides proof-of-concept support for the approach and its applicability to finding novel cancer cell-specific kinase addictions.

Predicted Kinases and Their Interaction Partners Formed Cell Type-Specific Signal Addiction Networks

The top KISS predictions turned out to form well-connected signaling networks consisting of both physical and functional interactions, suggesting that the individually most essential kinase targets play a role in shared biological processes. Focusing again on CAL51, we took a closer look at the interaction partners in the CAL51-centered network (Figure 5). The network analysis revealed that the KISS-predicted kinases formed a connected subnetwork with SYK as its main hub (Figure 5A; Table S6). SYK has been shown to regulate proliferation as a tumor suppressor, and inhibits breast cancer cell growth (Moroni et al., 2004; Sung et al., 2009). Furthermore, its early loss during progression of the disease was linked to poor prognosis and metastasis (Blancato et al., 2014; Toyama et al., 2003). Interestingly CAL51, a metastatic breast cancer cell line, had the lowest expression of *SYK* among all the tested cell lines (Barretina et al., 2012), raising the possibility that the observed growth inhibition upon targeting some of its interaction partners might be mediated by its reactivation. Importantly, siRNA knockdown of a number of significant kinase addiction predictions in the SYK-interactome showed marked growth inhibition (Figure 5B). The CAL51 addiction network was also highly enriched in several

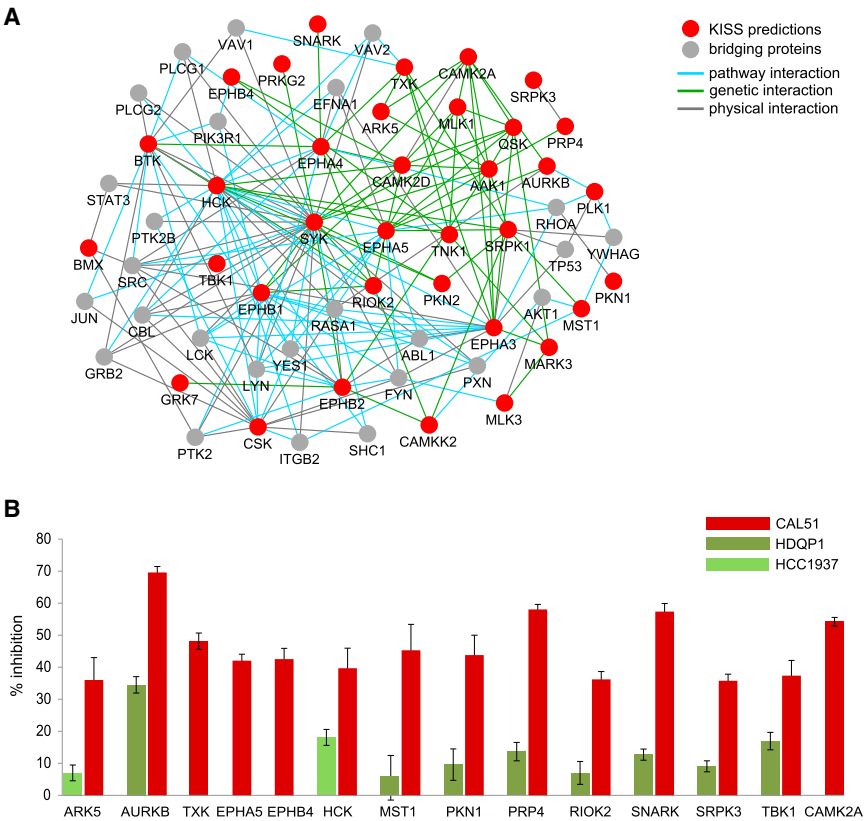

Figure 5. Integrative Network Analysis among the Strongest Kinase Addiction Predictions in CAL51

(A) The signal addiction network based on interactome analysis of the top predictions in CAL51 is highly connected with SYK as its most promiscuous hub. The high-confidence physical interactions occurring in breast neoplasm were extracted from the HIPPIE database for significant kinase addictions ($p < 0.06$). The GeneMania database was used to map the genetic interactions between the top predictions as well as pathway interactions involving the proteins in the network.

(B) Top kinase predictions validated by siRNA knockdown. Only hits with at least 35% average inhibition over the three replicates of the top two siRNA sequences are shown here, together with their error bars (SEM). Red bars represent the siRNA results in the CAL51 cell line, whereas green bars represent negative control cell lines, in which the KISS addiction prediction was insignificant (HDQP1 and HCC1937).

(C) Selected gene ontology biological processes that were highly enriched in the CAL51 signal addiction network ($p < 0.005$). The number of genes associated with a given GO term in the CAL51 network is marked beside the bars.

See Figure S2 for other cell line-specific networks and Table S6 for details of the interactions.

cancer-related gene ontology (GO) processes (Figure 5C; Table S6). An enrichment of several immune function and inflammation-related processes was also seen in the MDA-MB-436 and HDQP1 TNBC addiction networks (Figure S4). Notably, the toll-like receptor signaling pathway was among those enriched, consistent with previous studies showing the importance of this signaling pathway in breast tumor cell invasion, survival, and metastasis (Gonzalez-Reyes et al., 2010; Merrell et al., 2006; Yang et al., 2010).

KISS-Predicted Kinase Addictions Showed Consistency between Two Independent Compound Collections

We also evaluated the consistency of the kinase addiction scoring using a distinct panel of 295 kinase inhibitors from GlaxoSmithKline (GSK) (Knapp et al., 2013), which contains 87 shared kinase targets with our collection of 40 compounds (Figure 6A). Rankings of the shared kinases according to their KISS values, which were calculated based on drug responses in the two compound panels, revealed a significant association when applied to HER2-positive and ER-negative cell lines (Figure 6B; $p < 0.05$, Fisher's exact test) and an overlapping set of top functional addictions (Table S7). The significant overlap in the KISS profiles between these two distinct sets of kinase inhibitors is especially striking given the differences in their target selectivity profiling: the Institute for Molecular Medicine Finland (FIMM) compound targets were extracted from the competition binding assays (Davis et al., 2011), whereby dissociation constant (K_d) levels were estimated based on serial dilutions of a test compound across several concentrations, whereas the target annotations for the GSK compounds were extracted from two-dose testing in kinase assays (Knapp et al., 2013). This indicates that the kinase addiction predictions were not merely due to the compounds covered by our kinase inhibitor panel, but consistent addiction scores were obtained also when using an independent set of drug probes targeting the overlapping portion of the kinase space.

Combinatorial KISS Revealed Synergistic Drug Interactions and Co-essential Kinase Pairs

Since most cancer cells are dependent on multiple driver signals, we extended the KISS approach to also elucidate combinatorial molecular addictions, so-called druggable co-dependencies, in each cancer cell type individually. To predict synthetic lethal

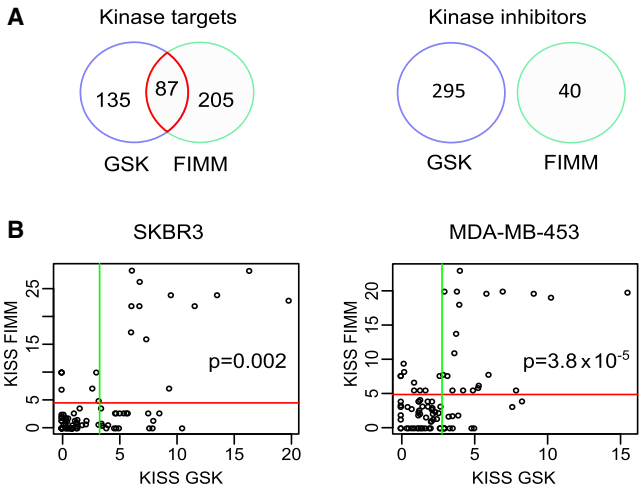

Figure 6. Comparison of the Top-Ranked Kinase Addictions between Two Independent Compound Collections

(A) Overlap of the kinase inhibitors and their kinase targets between the GSK and FIMM compound sets.

(B) Correlation of the KISS-based kinase rankings in two representative cell lines. KISS values were calculated for the 87 common kinase targets in the two non-overlapping drug sets (FIMM and GSK drug collections, Table S7). The resulting rankings revealed a common set of top signal addictions and were significantly correlated ($p < 0.05$, Fisher's exact test). Red and green lines indicate the average KISS level in the FIMM and GSK rankings, respectively, which were used as cut-off values in the contingency tables of the Fisher exact test for the association between the two rankings.

type interactions between kinase pairs, whose simultaneous inhibition leads to increased cancer cell death compared with the inhibition of each kinase individually, we first calculated the combinatorial KISS for all kinase target pairs in a given cell line, and then compared the predicted combination effect with those effects originating from inhibiting the single kinases alone (Figure 1A, right). We focused on those kinase pairs for which the combinatorial KISS was positive and exceeded the complement scores (here T = 4; see Figure 1B); these pairs were then ranked by the magnitude of their combinatorial KISS (Figure 7; Table S8). For the proof-of-concept validations, we chose the HCC1937 TNBC cell line, since it does not harbor any strong single driver addictions, thereby being a good model system for testing novel combinatorial treatment alternatives.

We hypothesized that the compounds which are the strongest non-common inhibitors of each individual kinase in the highly ranked kinase pairs should show a degree of synergism. To test this hypothesis, we paired the most potent inhibitors of the single kinases (Figure 7); these compound pairs were experimentally tested for their combined efficacy in the selected cell line in increasing inhibitor concentrations. Since some of the kinases were targeted by only a single compound, which sometimes was shared among several selected kinase targets, there were a number of kinase pairs (and thus compound pairs) with the same combinatorial KISS value, originating from their common inhibitors (the colored panels in Figure 7). Notably, however, we confirmed experimentally that at least one compound pair in each such combinatorial KISS class resulted in a synergistic phenotype (the pairs in boldface in Figure 7). For each of these synergistic combinations of nintedanib with enzastaurin, bosutinib with pazopanib or foretinib, and dasatinib with axitinib, the observed joint growth inhibition was markedly greater than the expected effect based on the Bliss independence model (Figures 8A and 8B), and greater than the combination effect observed in the self-crosses of these single agents (Table S9).

We further tested the predicted co-essential kinase pairs that led to synergistic compound combinations using siRNA-mediated target knockdown. We discovered that the majority of the selected kinase pairs (9 of 11 validated pairs, Figure 7) showed a co-essential phenotype, defined as higher combinatorial growth inhibition effect than that caused by each individual kinase when silenced alone. Strikingly, in seven out of these nine pairs, the combinatorial silencing effect was higher than 2-fold their expected effect (Figure 8C; Table S10). In particular, the kinase pairs predicted to underlie the synergistic compound effects (EPHB6 with AURKC, GCK with TAOK3 or CDK7, and GSK3b with PCTK1) were also shown to be co-essential. Taken together, these results suggest that the combinatorial KISS approach can identify unexpected synergistic interactions between compounds, which are often due to synthetic lethal type interactions between the kinase targets of the individual inhibitors that target distinct pathways (Table S11). This model hence explains the synergistic inhibition effect via a specific co-dependency pattern, in which the cancer cell is addicted to a number of kinase signals, each of which needs to be inhibited for maximal cancer cell killing.

DISCUSSION

We recently demonstrated how comprehensive testing of drug sensitivities in cells from leukemia patients may lead to unpredictable, clinically significant drug-repositioning opportunities, as well as to hypotheses about potential kinase-driven signaling networks to which the patient-derived cells may be addicted (Pemovska et al., 2013, 2015; Yadav et al., 2014). Once carefully tested, such network-based approaches could facilitate clinical decision making by means of mapping the key oncogenic signals underlying both the initial treatment sensitivity and acquired resistance during the disease evolution.

In the present study, we developed and tested a systematic chemical systems biology tool to explore druggable cancer addictions, both single kinase targets and their synthetic lethal type combinations, through integrating functional perturbation profiles from cell-based drug sensitivity assays and drug-target information from biochemical target selectivity assays. In an application to 40 kinase inhibitors, which span the target network among 205 kinases, we demonstrated how this integrated approach enabled us to classify selective kinase addiction patterns across heterogeneous TNBC cell lines in agreement with their clinical subtypes while showing considerable variability between the heterogeneous breast cancer cells, hence pinpointing putative mechanisms of drug sensitivity and resistance in a context-specific manner. Using known oncogenic drivers, such as ERBB2/HER2, BRAF, and PIK3CA, we showed that our kinase addiction score improves the ranking of the molecular addictions in a subset of breast cancers known to be driven by these kinases. Our unsupervised approach not only identified known breast cancer drivers in a totally unbiased manner, but

Kinase$_1$	Kinase$_2$	cs(k_1)	n_1	cs(k_2)	n_2	KISS(k_1,k_2)	Common inhibitor	Strongest inhibitor$_1$	Strongest inhibitor$_2$
*GSK3b	CDKL2	5.42	1	0.00	1	20.33	SNS-032	Enzastaurin	Sorafenib
GSK3b	**PCTK1**	5.42	1	0.00	1	20.33	SNS-032	**Enzastaurin**	**Nintedanib**
CDK7	**GSK3b**	6.38	3	5.42	1	20.33	SNS-032	Foretinib	Enzastaurin
CDK7	**PCTK1**	6.38	3	0.00	1	20.33	SNS-032	Foretinib	Nintedanib
GCK	**CDK7**	9.20	1	6.78	3	19.14	Alvocidib	**Bosutinib**	**Foretinib**
GCK	**TAOK3**	9.20	1	3.11	2	19.14	Alvocidib	**Bosutinib**	**Pazopanib**
* GCK	TYK2	9.20	1	1.26	3	19.14	Alvocidib	Bosutinib	Ruxolitinib
CDK7	TAOK3	6.78	3	3.11	2	19.14	Alvocidib	Foretinib	Pazopanib
* CDK7	TYK2	6.78	3	1.26	3	19.14	Alvocidib	Foretinib	Ruxolitinib
*TAOK3	TYK2	3.11	2	1.26	3	19.14	Alvocidib	Pazopanib	Ruxolitinib
EPHB6	**AURKC**	1.91	7	0.00	1	10.07	Barasertib	**Dasatinib**	**Axitinib**
RET	**AURKC**	0.48	10	0.00	1	10.07	Barasertib	Foretinib	Axitinib
HIPK4	**AURKC**	0.00	2	0.00	1	10.07	Barasertib	Foretinib	Axitinib
FLT3	AURKC	1.25	11	0.00	1	10.07	Barasertib	Sunitinib	Axitinib
MEK5	**AURKC**	0.62	5	0.00	1	10.07	Barasertib	Vemurafenib	Axitinib

Figure 7. Combinatorial KISS Results in the HCC-1937 Cell Line

The combinatorial KISS was calculated for a particular kinase pair (k_1, k_2) by averaging the drug response (DSS) over their common inhibitors that target both k_1 and k_2 (see Figure 1). The different background color panels indicate the sets of kinases (and compound pairs), which were indistinguishable by the current compound-target mappings. Boldface font indicates those compound and kinase pairs for which we have experimental support from compound and/or siRNA testing for being either synergistic or co-essential, respectively, and an asterisk indicates that the kinase pairs that were not experimentally tested in the present study.

also predicted a number of novel druggable addictions, including SNARK, ARK5, CAMK2A, SRMS, and PKN1. Experimental validations using both compound and siRNA combinations demonstrated that the model also successfully predicted a number of co-essential kinase pairs and synergistic kinase inhibitor combinations in the basal-like HCC1937 TNBC cell line, such as dasatinib with axitinib, enzastaurin with nintedanib, as well as bosutinib with pazopanib or foretinib, in which the combined inhibition power could not be explained by the efficacy of the two single compounds when used alone. Even though several of these compounds are currently not yet approved, their overlapping polypharmacology helped the network model to identify unexpected synergistic combinations regardless of their approval status (Table S1). Although we sometimes observed synergies at rather high concentrations, which may not be clinically feasible, the current proof-of-concept results could be further improved with an increasing knowledge of the drug-target selectivity. The present study focused on kinase inhibitors, due to their importance in anticancer drug development (Apsel et al., 2008; Fedorov et al., 2010) and the availability of comprehensive target selectivity profiles (Davis et al., 2011), but the chemical systems biology approach is applicable to any sets of compounds with known and partly overlapping target profiles.

Perhaps the biggest limitation of any target deconvolution method comes from the lack of comprehensive and accurate target annotations for many targeted compounds. Consequently, multiple kinases tended to obtain the same KISS value (e.g. all those targets having the same set of inhibitors in a given cell line). Experimental testing of these predictions is essential to discriminate the potential false positives. Similarly, since the joint inhibition of kinase pairs by the same set of drugs results in equal scoring from the combinatorial KISS, the compound combination rankings may also have ties (i.e. multiple kinase pairs explaining the efficacy of their common set of inhibitors). In our experimental validations, we were able to confirm one synergistic compound pair in each of the combinatorial KISS classes (Figure 7; Figures 8A and 8B). However, it is likely that an increased number of kinase inhibitors with overlapping target spaces will lead to more high-resolution predictions in the future. Furthermore, experimental issues may lead to some false-negative findings, i.e. lowly ranked kinases that are important for the cancer cell survival, for instance, due to the relatively short assessment time of drug sensitivity (in this case, 3 days), which may be insufficient to affect the viability readout. In addition, an efflux transporter effect may mask sensitivity to a kinase inhibitor, and thereby the addiction to the kinase function could remain undetected in compound phenotypic testing. However, our siRNA knockdown validation experiments gave complementary support for the essentiality of the predicted kinases. As a future development, it might be useful to combine the chemical and RNAi-based perturbation experiments with genomic analyses to provide improved identification of molecular addictions and co-dependencies, along the lines suggested in recent integrative studies (Gatza et al., 2014; Sundaramurthy et al., 2014; Vizeacoumar et al., 2013).

In summary, our integrated phenotype-based strategy provides complementary information compared with cancer sequencing efforts, which have their limitations in translating the genomic aberration into clinically actionable therapeutic strategies. For instance, even when causal aberrations can be identified, these are often pharmaceutically non-targetable, and even if druggable genetic alterations can be found, targeting them in the clinic often proves ineffective because of redundant activated driver signals or adaptive compensatory signaling. Compared with the genomic-based approaches (Aksoy et al., 2014; Tan et al., 2012), our functional approach does not require any background knowledge of the genetic alterations or other molecular biomarkers to elucidate potential therapeutic strategies. This may make it more straightforward to translate the most actionable predictions into a clinical setup, based solely on the ex vivo response of patient cells to a collection of drugs with known target annotations. The synergistic effects of drug combinations predicted by the combinatorial KISS suggest that this approach can identify new unexpected treatment strategies that modulate multiple, redundant, or compensatory signaling pathways. Finally, our results warrant the development of improved inhibitors with higher dual potency and selectivity

A

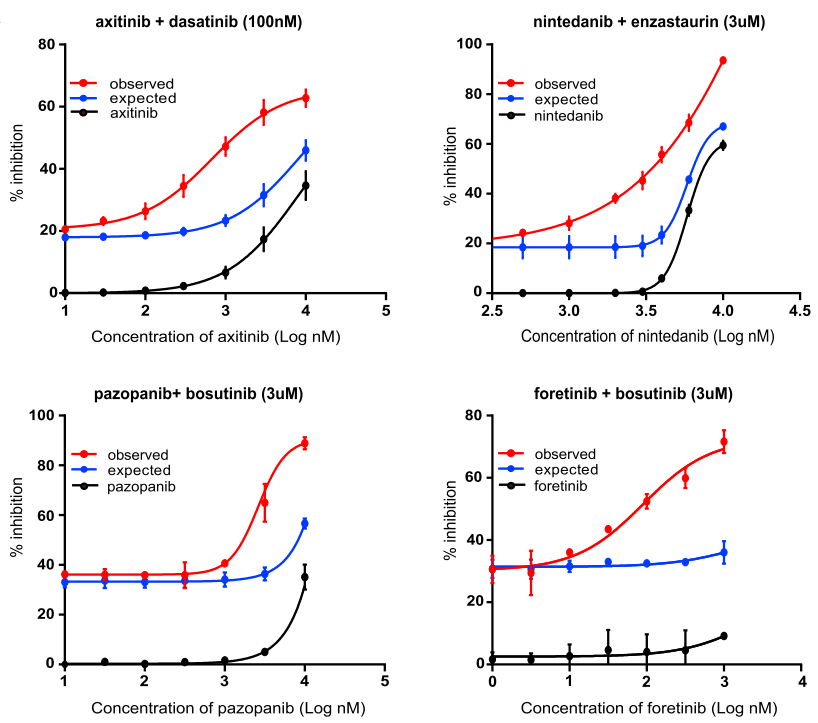

B

axitinib \ dasatinib

axitinib \ dasatinib	0	1	3	10	30	100	300	1000
0	0.00	0.00	0.00	0.01	0.13	15.31	53.60	63.81
10	0.04	0.18	0.44	1.35	3.79	20.75	47.57	67.41
30	0.12	0.31	0.66	1.87	5.07	23.64	49.99	67.03
100	0.40	0.65	1.03	2.50	6.41	27.01	52.28	67.76
300	1.19	1.47	1.49	2.16	5.57	37.73	62.67	67.10
1000	3.95	6.98	7.85	11.97	21.95	49.36	67.82	75.49
3000	11.55	21.57	22.86	28.58	40.06	62.07	74.37	81.00
10000	36.79	46.00	47.08	48.94	53.30	66.52	79.94	99.38

axitinib \ dasatinib

axitinib \ dasatinib	0	1	3	10	30	100	300	1000
0								
10		0.00	0.00	0.01	0.04	0.05	-0.06	0.04
30		0.00	0.01	0.02	0.05	0.08	-0.04	0.03
100		0.00	0.01	0.02	0.06	0.11	-0.02	0.04
300		0.00	0.00	0.01	0.04	0.21	0.09	0.03
1000		0.03	0.04	0.08	0.18	0.31	0.12	0.10
3000		0.10	0.11	0.17	0.28	0.37	0.15	0.13
10000		0.09	0.10	0.12	0.16	0.20	0.09	

foretinib \ bosutinib

foretinib \ bosutinib	0	500	1000	2000	3000	4000	6000	10000
0	0.02	0.41	1.56	6.55	32.84	62.36	87.96	96.45
1	0.00	0.01	0.20	5.19	33.68	61.66	87.79	95.78
3	0.00	0.02	0.27	6.61	34.52	62.52	88.40	97.18
10	0.00	0.00	0.08	7.25	36.48	67.46	88.83	95.08
30	0.00	0.07	0.81	15.25	43.63	68.66	88.46	96.86
100	0.00	0.13	1.42	24.94	54.06	74.77	89.14	96.12
300	0.00	1.67	9.29	38.08	62.16	76.30	84.64	93.36
1000	8.52	7.65	31.50	58.08	74.24	83.42	88.21	98.75

foretinib \ bosutinib

foretinib \ bosutinib	0	500	1000	2000	3000	4000	6000	10000
0								
1		0.00	-0.01	-0.01	0.01	-0.01	0.00	-0.01
3		0.00	-0.01	0.00	0.02	0.00	0.00	0.01
10		0.00	-0.01	0.01	0.04	0.05	0.01	-0.01
30		0.00	-0.01	0.09	0.11	0.06	0.01	0.00
100		0.00	0.00	0.18	0.21	0.12	0.01	0.00
300		0.01	0.08	0.32	0.29	0.14	-0.03	-0.03
1000		-0.01	0.22	0.44	0.36	0.18	-0.01	

C

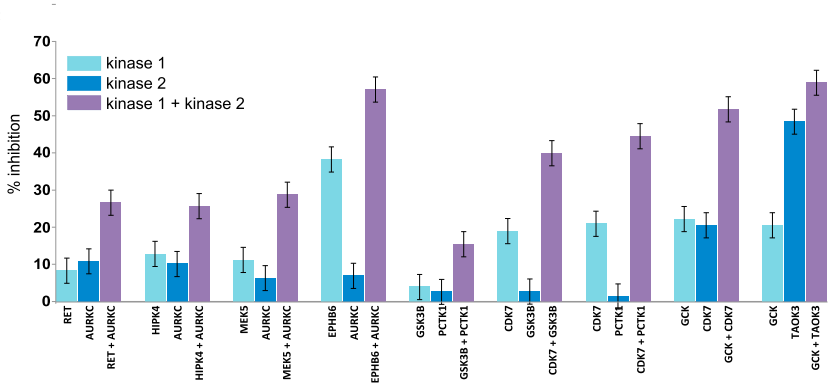

Figure 8. Combinatorial KISS Predicts Synergistic Compound Combinations and Co-essential Kinase Pairs

(A) Dose-response curves for the synergistic inhibitor effects on cell viability in HCC1937. Each combination was tested in two to four replicates. Points and error bars represent the mean and its SE, respectively, and the solid curve is the logistic function fit. The expected combinatorial effects were calculated based on the Bliss independence model (Bliss, 1956).

(B) Examples of the full dose-response matrices showing the effects of the synergistic compound combinations on the cell viability (left) and their Bliss excess scores (right).

(C) Effects of single and combinatorial siRNA knockdowns of the top kinase pairs on HCC-1937 cell viability. Three siRNAs per gene were tested both in a 3 × 3 matrix format (combination effects) and alone (single effects) in three replicates. Bars and error bars represent percent inhibition and SE after single and combinatorial siRNA knockdown of the selected pairs. For scoring of co-essentiality, the maximum single effect was used as the baseline comparison level for the combination effect.

Tables S8, S9, S10, and S11 provide the full data.

toward the top target pairs, which could further improve the treatment efficacy as shown earlier (Dar et al., 2012). We envision that iterative experimental drug sensitivity testing followed by combinatorial KISS analyses and chemical optimization could offer a powerful means for phenotype-driven development of new, highly disease subtype-selective drug leads.

SIGNIFICANCE

This proof-of-principle study demonstrates how integration of kinase inhibitor perturbation screens with computational target deconvolution approaches offers possibilities to elucidate both mono- and multi-targeted molecular addictions in individual cancer cells. As broad-scale drug sensitivity testing is becoming a commonly used approach to functionally profile both cancer cell lines and patient-derived cancer cells, our integrated platform can greatly benefit many chemical, biological, and clinical applications. Integration of comprehensive chemical screening and target selectivity profiling provides improved understanding of the biological mechanisms behind drug sensitivity and resistance in individual cancer types and patients. Experimentally, our approach enables computational prediction of synergistic target and drug pairs, which may help to prioritize and speed up the experimental testing of the massive number of potential combinations. Personalized medicine programs should also benefit from the systematic mapping of oncogenic driver signals and pharmaceutically actionable molecular addictions during cancer progression and relapse, as well as from the possibility to predict next-line, combination therapeutic opportunities that are tailored for the individual, relapsed patient.

EXPERIMENTAL PROCEDURES

Cell Line Material

The characteristics of the breast cancer cell lines, including their vendors and culturing conditions, are detailed in Table S2.

Drug Sensitivity Screening

The sensitivity of the 21 breast cancer cell lines to 239 anticancer compounds was tested using the DSRT platform (Pemovska et al., 2013). Each compound was tested in five concentrations, across a 10,000-fold range, allowing for the establishment of dose-response curves and their subsequent quantification by IC_{50} and the DSS (Yadav et al., 2014). The DSS values of the compounds and their clinical status are provided in Table S1. Differential DSS and IC_{50} values were calculated using either the mean over all cell lines or the MCF10A cell line as a control. The same protocol was used for testing the GSK compounds in the MDA-MD-453 and SKBR3 cell lines. An independent set of drugs used in validations of the KISS predictions was tested in selected cell lines using eight concentrations over a 10,000-fold range (see Independent Drug and siRNA Testing). The predicted drug synergies were tested in an 8 × 8 dose-matrix format (see Combinatorial Drug Synergy Testing).

Drug-Target Mappings

As a source of quantitative drug-target data, we used the biochemical competition binding study performed by Davis et al. (2011), where the K_d values for 205 non-mutated kinases were available for 40 inhibitors from our FIMM drug collection. Drug targets were defined using drug-specific K_d thresholds (50-fold from the strongest target of a given inhibitor or below 100 nM, whichever threshold came first), followed by an expert manual curation, resulting in a quantitative drug-target dataset (qDT, Table S3).

As a source of non-quantitative, unary drug-target data (uDT), we combined kinases listed as targets in KEGG (http://www.genome.jp/kegg), the Therapeutic Target Database (http://bidd.nus.edu.sg/group/cjttd), and DrugBank (http://www.drugbank.ca). This resulted in 296 kinase targets for 142 drugs in our FIMM drug collection (Table S3). Such unary target selectivity data specify which kinases have been reported as targets of a given drug, but lack the information about those not being reported as a target or not being tested.

For the GSK compounds, we used the kinase activity assay from Knapp et al. (2013), available in ChEMBL (https://www.ebi.ac.uk/chembl/), where the kinases were subdivided into five categories (from 0, inactive to 4, very active), based on the inhibition of their activity at 1 and 0.1 μM concentrations of a particular compound, according to pre-defined thresholds. Kinases classified into categories 3 and 4 were considered to be targets of the GSK compounds. Kinases belonging to category 2 were considered to be targets only if the compound had no targets in higher categories.

Kinase Addiction Predictions

To make a systematic comparison of the KISS approach with previous methods, we ranked the kinase targets using the drug response profiles in each cell line based on Tyner's score (Tyner et al., 2013), Fisher's test (Wei et al., 2012), and Spearman's correlation (Tran et al., 2014). In the Tyner score method, kinases from the quantitative drug-target data for each drug were subdivided into five tiers depending on the magnitude of their K_d or IC_{50} value (Tyner et al., 2013). Each kinase was then assigned a cumulative score, resulting from addition of points (its effective inhibitors) and subtraction of points (its ineffective inhibitors).

In the Fisher test method, a p value for each kinase was calculated based on the number of its active inhibitors, active non-inhibitors, inactive inhibitors, and inactive non-inhibitors (Wei et al., 2012). The active drugs were defined to be among the top 20% of the most effective drugs in a given cell line. In the Spearman correlation method, the kinases were ranked based on the correlation between drug response and the kinase selectivity profile in each cell line separately. The Fisher test and Spearman correlation-based methods were tested with quantitative drug-target data (qDT) and two types of drug response data (IC_{50} or DSS). In addition, we tested both non-differential and differential versions of IC_{50} and DSS (see the explanation in Drug Sensitivity Screening). Altogether we examined 31 technically possible combinations of the deconvolution method, drug response data, and drug-target data, each resulting in a separate ranking of kinase targets (Table S4).

Comparison of the Kinase Addiction Predictions

To evaluate the kinase target rankings resulting from the different approaches, we extracted the ranks of known kinase drivers (ERBB2/HER2, BRAF, and PIK3CA/PI3Kα) in seven of the cell lines as positive controls, and calculated their median rank across these cell lines. The mutations of *PIK3CA* and *BRAF* in breast cancer cells were extracted from the COSMIC database (as of June 2012; http://cancer.sanger.ac.uk/). Only cell lines harboring a mutation that had an impact on the protein function were used in the evaluation. The functional impact was assessed using the IntOGen database (as of March 2013; http://beta.intogen.org/web/cell-lines).

Statistical Significance of a KISS Value

To assess the statistical significance of an observed KISS value, we determined the empirical p values using permutations tests. More specifically, a vector consisting of numbers of inhibitors per kinase was used to randomly select a given number of inhibitors for each kinase, whose drug response values in a given cell line were then averaged. In other words, the links in the drug-target network were randomly re-ordered while preserving the overall distribution of the number of inhibitors per kinase. The permutation procedure was repeated, simulating at least 10,000 random KISS values in a given cell line. The empirical p value was defined by the percentage of the permuted KISS values above or equal to the observed one (Table S4).

Construction of Addiction Networks

The CAL51 addiction network was constructed using the high-confidence interactions, both physical and associations, in breast neoplasm for the top KISS predictions from the HIPPIE database (http://cbdm.mdc-berlin.de/tools/hippie), where only the interactors connected with at least three input proteins were

retained. The resulting network was further populated using pathway and genetic links extracted from GeneMania (http://www.genemania.org). For visualization purposes, genetic interactions with less than two proteins from the top KISS predictions were filtered out. The network was visualized using Cytoscape v.3.0.1. Enrichment of GO biological processes was analyzed using ClueGo v.2.8 (Bindea et al., 2009), with the minimum number and percentage of genes per term being set to 4 and 2, respectively, and the Benjamini Hochberg method applied as the p value correction method (Table S6).

Independent Drug and siRNA Testing

The top single KISS predictions were tested in selected cell lines using both siRNA knockdowns and an independent set of kinase inhibitors. The predictions from MDA-MD-436 and DU4475 cell lines were tested using independent drugs only, whereas the predictions from HDQP1, Hs578T, and CAL51 were tested using drugs and/or siRNAs, depending on the kinase target. As additional drugs we chose those that had the lowest K_d values for the kinase in question (Davis et al., 2011), but were not previously tested in the FIMM drug set used to generate the KISS predictions. These independent drugs were ordered from MedChemexpress and tested in the same way as described above (Drug Sensitivity Screening). siRNA validations were performed using three siRNA sequences per kinase individually at a concentration of 10 nM and tested in three replicates in the cell lines predicted to be positive and negative for each kinase addiction. The siRNAs for the kinases as well as for the positive and negative controls were ordered from Ambion and tested using the same protocol as described below (siRNA Combination Testing) with 750 cells per well for all cell lines, except for HCC1937 and BT549 whereby 500 cells per well were used. The number of cells for plating was determined based on the transfection optimization experiments. Fluorescence values were converted to percent inhibition using positive and negative controls. The average siRNA knockdown was calculated for each sequence based on the three replicates, and the two highest means were further averaged to result in the final siRNA inhibition score. Kinases whose final siRNA inhibition score was $\geq$35% were considered as positively validated. For the independent drug tests, we considered DSS $\geq$7 as an indication of a positive validation (Table S5).

Combinatorial KISS Predictions

The combinatorial KISS score was calculated for all kinase pairs that had common inhibitor(s) as well as individual inhibitors among the 40 kinase inhibitors in common between our FIMM drug collection and the selectivity profiling assays (Davis et al., 2011). Kinase pairs that had no common inhibitors or no single kinase inhibitors in our compound collection were excluded from the combinatorial analysis. Next, to focus on synthetic lethal type of kinase pairs, termed co-essential, we excluded all those pairs for which the difference between the combinatorial KISS and the complement scores was below a selected cut-off value (here T = 4, see Figure 1). The remaining kinase pairs were ranked by the magnitude of their combinatorial KISS and mapped back to drug pairs by selecting the strongest inhibitors of kinases 1 and 2 alone, excluding their common inhibitors, using the lowest K_d values (Davis et al., 2011) (Table S8). The top co-essential kinase pairs predicted by the combinatorial KISS, as well as the corresponding drug pairs of their individual inhibitors, were experimentally tested in HCC1937 cells as described below.

Combinatorial Drug Synergy Testing

To test the combinatorial KISS predictions, the top-ranked drug combinations in the HCC1937 cell line were tested in an 8 × 8 dose-matrix format covering seven increasing concentrations of each drug, along with all their pairwise combinations, as well as the negative control (0.1% DMSO, top left corner of the 8 × 8 matrix) and the cell-killing positive control (100 μM benzethonium chloride, bottom right corner of the matrix). Drugs were transferred in clear-bottom black 384 well plates (Corning) using an Echo 550 Liquid Handler (Labcyte) as per the matrix design. Liquid handling was performed using a MultiDrop Combi dispenser (Thermo Scientific). 5 μl of culture medium was dispensed in each well of pre-drugged plates to dissolve the drugs, and maintained in the orbital shaker for about 1 hr. Next, 20 μl of cell suspension (1,000 cells per 20 μl) was added to the drugged plates. After 72 hr of incubation at 37°C in 5% CO_2 in a humidified incubator, the cell viability was measured using CellTiter-Blue (Promega). 3 μl of CellTiter-Blue reagent was added to the plates, which were then incubated for 2 hr at 37°C. Fluorescence intensity (595 nm) was measured using a PheraStar FS plate reader (BMG Labtech). The raw intensity values were converted to percent inhibition using the plate average of positive and negative controls. Next, to reduce the dispensing-related experimental variation from well to well, each row and column from the 8 × 8 matrices was fitted in GraphPad Prism software using logistic model, and the two fitted values per well were then averaged. The expected combination effects were calculated on the basis of the Bliss independence model (Bliss, 1956) (Table S9).

siRNA Combination Testing

The top co-essential kinase pairs predicted by the combinatorial KISS in HCC1937 cells were tested in an siRNA combination assay. Three siRNAs per kinase were purchased from Qiagen and tested in 4 × 4 matrices, in which the top left corner was occupied by a control, and the remaining wells in the first row and column by single siRNAs (at 8 nM) of the first and second kinase, respectively. All the pairwise combinations were tested in the remaining nine wells using 8 nM of each siRNA. SiRNAs were transferred to clear-bottom 384 well plates with the Echo 550 Liquid Handler. 5 μl of Opti-MEM (Life Technologies) containing 50 nl of Lipofectamine RNAiMAX Transfection Reagent (Life Technologies) was added to each well of pre-siRNA-coated plates using an MultiDrop Combi nl dispenser (Thermo Scientific) and incubated at room temperature for 20 min on an orbital shaker. 20 μl of cell suspension (500 cells per 20 μl) were seeded on the siRNA plate and the plates were maintained at 37°C, in the presence of 5% CO_2 in a humidified incubator for 96 hr. CellTiter-Glo (Promega) reagent was then used to assess the viability of cells after siRNA treatments. *Z* prime scores were calculated for each plate, and these remained above 0.5, assuring good resolution. The fluorescence measurements were converted to percent inhibition using the mean fluorescence of 16 positive and 24 negative controls. The single siRNA knockdown effects were normalized by taking the average of the inhibition values of single kinase knockdown and those double kinase knockdown that included this kinase with lower inhibition values, to make the single and double kinase knockdown results comparable. Maximum single siRNA knockdown effect was considered to be the expected combinatorial effect in the absence of established synergy scoring (see also Table S10).

SUPPLEMENTAL INFORMATION

Supplemental Information includes two figures and 11 tables and can be found with this article online at http://dx.doi.org/10.1016/j.chembiol.2015.06.021.

AUTHOR CONTRIBUTIONS

A.S. designed and performed data analysis, and wrote the manuscript. P.G. coordinated and performed the experimental work, and assisted in writing the manuscript. L.K., S.K.J., J.S., and L.T. assisted in performing the experiments. S.S., B.Y., and J.T. analyzed the data. K.W. conceived and managed the project, and assisted in writing the manuscript. T.A. conceived and managed the project, and wrote the manuscript. All of the authors approved the final manuscript.

ACKNOWLEDGMENTS

The authors acknowledge and thank Karoliina Laamanen, Dr. Carina von Schantz-Fant, Katja Suomi, and Elina Huovari from the High Throughput Biology Unit at FIMM, as well as Arjan van Adrichem for their great technical assistance and help in performing the drug screening and siRNA testing experiments. The authors also thank Tea Pemovska for useful discussions and Dr. Milla Kibble for checking the language. This study was financially supported by the Academy of Finland (grants 269 862, 272 437, 277 293, and 279 163), Helsinki Biomedical Graduate Program (HBGP), the Cancer Society of Finland, Biomedicum Helsinki Foundation, Biocenter Finland, and Jane and Aatos Erkko Foundation.

Received: March 20, 2015
Revised: June 2, 2015
Accepted: June 15, 2015
Published: July 23, 2015

REFERENCES

Aksoy, B.A., Demir, E., Babur, O., Wang, W., Jing, X., Schultz, N., and Sander, C. (2014). Prediction of individualized therapeutic vulnerabilities in cancer from genomic profiles. Bioinformatics *30*, 2051–2059.

Apsel, B., Blair, J.A., Gonzalez, B., Nazif, T.M., Feldman, M.E., Aizenstein, B., Hoffman, R., Williams, R.L., Shokat, K.M., and Knight, Z.A. (2008). Targeted polypharmacology: discovery of dual inhibitors of tyrosine and phosphoinositide kinases. Nat. Chem. Biol. *4*, 691–699.

Barretina, J., Caponigro, G., Stransky, N., Venkatesan, K., Margolin, A.A., Kim, S., Wilson, C.J., Lehar, J., Kryukov, G.V., Sonkin, D., et al. (2012). The Cancer Cell Line Encyclopedia enables predictive modelling of anticancer drug sensitivity. Nature *483*, 603–607.

Bindea, G., Mlecnik, B., Hackl, H., Charoentong, P., Tosolini, M., Kirilovsky, A., Fridman, W.H., Pages, F., Trajanoski, Z., and Galon, J. (2009). ClueGO: a Cytoscape plug-in to decipher functionally grouped gene ontology and pathway annotation networks. Bioinformatics *25*, 1091–1093.

Blancato, J., Graves, A., Rashidi, B., Moroni, M., Tchobe, L., Ozdemirli, M., Kallakury, B., Makambi, K.H., Marian, C., and Mueller, S.C. (2014). SYK allelic loss and the role of Syk-regulated genes in breast cancer survival. PLoS One *9*, e87610.

Bliss, C.I. (1956). The calculation of microbial assays. Bacteriol. Rev. *20*, 243–258.

Dar, A.C., Das, T.K., Shokat, K.M., and Cagan, R.L. (2012). Chemical genetic discovery of targets and anti-targets for cancer polypharmacology. Nature *486*, 80–84.

Davis, M.I., Hunt, J.P., Herrgard, S., Ciceri, P., Wodicka, L.M., Pallares, G., Hocker, M., Treiber, D.K., and Zarrinkar, P.P. (2011). Comprehensive analysis of kinase inhibitor selectivity. Nat. Biotechnol. *29*, 1046–1051.

Fedorov, O., Muller, S., and Knapp, S. (2010). The (un)targeted cancer kinome. Nat. Chem. Biol. *6*, 166–169.

Garraway, L.A., and Lander, E.S. (2013). Lessons from the cancer genome. Cell *153*, 17–37.

Gatza, M.L., Silva, G.O., Parker, J.S., Fan, C., and Perou, C.M. (2014). An integrated genomics approach identifies drivers of proliferation in luminal-subtype human breast cancer. Nat. Genet. *46*, 1051–1059.

Gonzalez-Reyes, S., Marin, L., Gonzalez, L., Gonzalez, L.O., del Casar, J.M., Lamelas, M.L., Gonzalez-Quintana, J.M., and Vizoso, F.J. (2010). Study of TLR3, TLR4 and TLR9 in breast carcinomas and their association with metastasis. BMC Cancer *10*, 665.

Grigoriadis, A., Mackay, A., Noel, E., Wu, P.J., Natrajan, R., Frankum, J., Reis-Filho, J.S., and Tutt, A. (2012). Molecular characterisation of cell line models for triple-negative breast cancers. BMC Genomics *13*, 619.

Heiser, L.M., Sadanandam, A., Kuo, W.L., Benz, S.C., Goldstein, T.C., Ng, S., Gibb, W.J., Wang, N.J., Ziyad, S., Tong, F., et al. (2012). Subtype and pathway specific responses to anticancer compounds in breast cancer. Proc. Natl. Acad. Sci. USA *109*, 2724–2729.

Hopkins, A.L. (2008). Network pharmacology: the next paradigm in drug discovery. Nat. Chem. Biol. *4*, 682–690.

Huang, M., Shen, A., Ding, J., and Geng, M. (2014). Molecularly targeted cancer therapy: some lessons from the past decade. Trends Pharmacol. Sci. *35*, 41–50.

Knapp, S., Arruda, P., Blagg, J., Burley, S., Drewry, D.H., Edwards, A., Fabbro, D., Gillespie, P., Gray, N.S., Kuster, B., et al. (2013). A public-private partnership to unlock the untargeted kinome. Nat. Chem. Biol. *9*, 3–6.

Lehmann, B.D., Bauer, J.A., Chen, X., Sanders, M.E., Chakravarthy, A.B., Shyr, Y., and Pietenpol, J.A. (2011). Identification of human triple-negative breast cancer subtypes and preclinical models for selection of targeted therapies. J. Clin. Invest. *121*, 2750–2767.

Merrell, M.A., Ilvesaro, J.M., Lehtonen, N., Sorsa, T., Gehrs, B., Rosenthal, E., Chen, D., Shackley, B., Harris, K.W., and Selander, K.S. (2006). Toll-like receptor 9 agonists promote cellular invasion by increasing matrix metalloproteinase activity. Mol. Cancer Res. *4*, 437–447.

Moroni, M., Soldatenkov, V., Zhang, L., Zhang, Y., Stoica, G., Gehan, E., Rashidi, B., Singh, B., Ozdemirli, M., and Mueller, S.C. (2004). Progressive loss of Syk and abnormal proliferation in breast cancer cells. Cancer Res. *64*, 7346–7354.

Pe'er, D., and Hacohen, N. (2011). Principles and strategies for developing network models in cancer. Cell *144*, 864–873.

Pemovska, T., Kontro, M., Yadav, B., Edgren, H., Eldfors, S., Szwajda, A., Almusa, H., Bespalov, M.M., Ellonen, P., Elonen, E., et al. (2013). Individualized systems medicine strategy to tailor treatments for patients with chemorefractory acute myeloid leukemia. Cancer Discov. *3*, 1416–1429.

Pemovska, T., Johnson, E., Kontro, M., Repasky, G.A., Chen, J., Wells, P., Cronin, C.N., McTigue, M., Kallioniemi, O., Porkka, K., et al. (2015). Axitinib effectively inhibits BCR-ABL1(T315I) with a distinct binding conformation. Nature *519*, 102–105.

Sundaramurthy, V., Barsacchi, R., Chernykh, M., Stoter, M., Tomschke, N., Bickle, M., Kalaidzidis, Y., and Zerial, M. (2014). Deducing the mechanism of action of compounds identified in phenotypic screens by integrating their multiparametric profiles with a reference genetic screen. Nat. Protoc. *9*, 474–490.

Sung, Y.M., Xu, X., Sun, J., Mueller, D., Sentissi, K., Johnson, P., Urbach, E., Seillier-Moiseiwitsch, F., Johnson, M.D., and Mueller, S.C. (2009). Tumor suppressor function of Syk in human MCF10A in vitro and normal mouse mammary epithelium in vivo. PLoS One *4*, e7445.

Tan, H., Bao, J., and Zhou, X. (2012). A novel missense-mutation-related feature extraction scheme for 'driver' mutation identification. Bioinformatics *28*, 2948–2955.

Tang, J., and Aittokallio, T. (2014). Network pharmacology strategies toward multi-target anticancer therapies: from computational models to experimental design principles. Curr. Pharm. Des. *20*, 23–36.

Torkamani, A., Verkhivker, G., and Schork, N.J. (2009). Cancer driver mutations in protein kinase genes. Cancer Lett. *281*, 117–127.

Toyama, T., Iwase, H., Yamashita, H., Hara, Y., Omoto, Y., Sugiura, H., Zhang, Z., and Fujii, Y. (2003). Reduced expression of the Syk gene is correlated with poor prognosis in human breast cancer. Cancer Lett. *189*, 97–102.

Tran, T.P., Ong, E., Hodges, A.P., Paternostro, G., and Piermarocchi, C. (2014). Prediction of kinase inhibitor response using activity profiling, in vitro screening, and elastic net regression. BMC Syst. Biol. *8*, 74.

Tyner, J.W., Yang, W.F., Bankhead, A., 3rd, Fan, G., Fletcher, L.B., Bryant, J., Glover, J.M., Chang, B.H., Spurgeon, S.E., Fleming, W.H., et al. (2013). Kinase pathway dependence in primary human leukemias determined by rapid inhibitor screening. Cancer Res. *73*, 285–296.

Vandin, F., Upfal, E., and Raphael, B.J. (2012). De novo discovery of mutated driver pathways in cancer. Genome Res. *22*, 375–385.

Vizeacoumar, F.J., Arnold, R., Vizeacoumar, F.S., Chandrashekhar, M., Buzina, A., Young, J.T., Kwan, J.H., Sayad, A., Mero, P., Lawo, S., et al. (2013). A negative genetic interaction map in isogenic cancer cell lines reveals cancer cell vulnerabilities. Mol. Syst. Biol. *9*, 696.

Wei, X., Hoffman, A.F., Hamilton, S.M., Xiang, Q., He, Y., So, W.V., So, S.S., and Mark, D. (2012). A simple statistical test to infer the causality of target/phenotype correlation from small molecule phenotypic screens. Bioinformatics *28*, 301–305.

Xie, L., Xie, L., Kinnings, S.L., and Bourne, P.E. (2012). Novel computational approaches to polypharmacology as a means to define responses to individual drugs. Annu. Rev. Pharmacol. Toxicol. *52*, 361–379.

Yadav, B., Pemovska, T., Szwajda, A., Kulesskiy, E., Kontro, M., Karjalainen, R., Majumder, M.M., Malani, D., Murumagi, A., Knowles, J., et al. (2014). Quantitative scoring of differential drug sensitivity for individually optimized anticancer therapies. Sci. Rep. *4*, 5193.

Yang, H., Zhou, H., Feng, P., Zhou, X., Wen, H., Xie, X., Shen, H., and Zhu, X. (2010). Reduced expression of Toll-like receptor 4 inhibits human breast cancer cells proliferation and inflammatory cytokines secretion. J. Exp. Clin. Cancer Res. *29*, 92.

Zhao, S., and Iyengar, R. (2012). Systems pharmacology: network analysis to identify multiscale mechanisms of drug action. Annu. Rev. Pharmacol. Toxicol. *52*, 505–521.